Numerical study of high impedance T-match antennas for terahertz photomixers

JUUL, Lars, MIKULICS, Martin, PEREIRA, Mauro <http://orcid.org/0000-0002-2276-2095> and MARSO, Michel

Numerical Study of High Impedance T-match Antennas for Terahertz Photomixers

Lars Juul · Martin Mikulics · Mauro F. Pereira · Michel Marso

Abstract This paper outlines an efficient numerical method to design terahertz photomixers. The simulations are benchmarked using measured power levels from results published in the literature. Next, the method is applied to two new photomixer designs based on the high impedance T-match antenna with bias supply DC-blocking structures for either a uniplanar layout or a multilayer structure for improved device reliability. Manufacturability is favoured by avoiding the use of airbridges, substrate thinning or under-etching. The estimated output power of the improved design is $9.0\,\mu$W, which is an improvement of 3 times over the reference photomixer.

Keywords Photoconductor Impedance · Terahertz Photomixer · Numerical Simulation · T-match Antenna

1 Introduction

Commercial applications of terahertz technology are inhibited by a lack of compact, inexpensive tunable sources with a large dynamic range for continuous wave (CW) spectroscopy and imaging purposes. THz Quantum cascade lasers (QCLs) (Köhler et al, 2002) already deliver over 1 W of pulsed power (Li et al, 2014). However they require cryocooling, e.g. for 3.4 THz emission this record laser has a maximum operating temperature of 123 K. Examples of single-mode coherent

L. Juul, M. Marso
Université Du Luxembourg, Research Unit for Engineering Science, L-1359 Luxembourg, Luxembourg
E-mail: lars.juul@uni.lu; michel.marso@uni.lu

M. Mikulics
Peter Grünberg Institute (PGI-9), Forschungscentrum Jülich, D-52425 Jülich, Germany
E-mail: M.Mikulics@fz-juelich.de

M. Pereira
Sheffield Hallam University, Materials and Engineering Research Institute, Sheffield S1 1WB, United Kingdom
E-mail: M.Pereira@shu.ac.uk

QCLs include (Kumar, 2011) with 2 mW output power at 1.8 THz and 155 K and (Ravaro et al, 2013) with 2 mW at 2.5 THz and 20 K. QCLs are extremely expensive and their predicitive design requires advanced mathematical physics approaches, such as Nonequilibrium Greens Functions Theories (Schmielau and Pereira, 2009c,a,b; Wacker et al, 2013).

Resonant tunneling diode (RTD) oscillators have made significant progress towards the production of a high power source in the terahertz region, with 10 μW at 1.31 THz (Asada and Suzuki, 2013). The device consists of and AC-coupled multilayer slot antenna with a parasitic bismuth resistor structure and a 12-layer GaInAs/AlAs double-barrier RTD on a semi-insulating InP substrate. The oscillation frequency is defined by the slot antenna resonator and the RTD parasitics, with no tunability option.

Terahertz sources based on frequency multiplier chains have become commercially available from companies such as Virginia Diodes, Inc. The sources deliver more than 10 μW output power up to 3 THz with a tuning range of 10% of the centre frequency (Drouin et al, 2013). The single elements in the multiplier chain are based on machined metal waveguides with flange sizes on the order of an inch and typically require separate bias voltage supplies. The bias voltages require careful tuning in order to avoid spurious oscillations, originating from the RF-blocking capacitors in the bias feeds (Drouin et al, 2013).

Low Temperature Grown (LT) GaAs photomixing technology is far from delivering the abovementioned power levels but it is a proven method and far less expensive to design and fabricate with only one epitaxial layer growth and one lift-off process for the metal pattern. It has the further advantage of room temperature operation (Mayorga et al, 2004) and wafer-level manufacturing scalability. A resonant LT GaAs photomixer was reported to generate 3 μW output power at 0.85 THz (Duffy et al, 2001). An output power of 2.6 μW at 0.85 THz was measured for a nitrogen-implanted GaAs (GaAs:N) travelling wave photomixer (Mikulics et al, 2006). An InGaAs/InP travelling wave uni-travelling carrier photodiode mixer (TW-UTC-PD) coupled to a resonant slot antenna with 1.55 μm optical sources has delivered 24 μW output power (Rouvalis et al, 2010). Semiconductor materials consisting of successive InGaAs and InAlAs quantum well structures have been grown with the intent to produce a bandgap suitable for THz generation with 1.55 μm telecom laser sources. Suitably low carrier lifetimes and high mobility values have been demonstrated for InGaAs/InAlAs, but the lower resistivity value, compared to LT GaAs, causes increased thermal noise and self-heating due to an increased dark current (Missous et al, 2013). Finally, several theoretical attempts to increase the photomixer output power through high impedance antenna designs have been made (Han et al, 2010; Juul et al, 2012).

The simplicity of heterodyne photomixers in concept and manufacturing, combined with the move towards less costly 1.55 μm telecom laser sources, make them a compelling option for room temperature CW sources.

This work describes the design of two new photomixer high impedance antenna structures, based on the T-match antenna by (Kraus and Sturgeon, 1940) with two options for DC-blocking structures. The layouts are deliberately following a low-risk design approach, avoiding the use of air bridges, substrate thinning, and under-etching, to favour manufacturability, reliability, and cost. The optimised devices can be applied directly for LT GaAs and GaAs:N technologies and can be

adapted to other substrate materials. The potential in high impedance resonant antennas for terahertz photomixers has yet to be fully exploited.

2 Outline of the Numerical Method

One of the technology specific challenges for the heterodyne photomixer is the low terahertz current delivered to the antenna. The terahertz current, i_{thz}, for a given optical beat frequency, ω, can found using the AC-responsivity relation given by (Mikulics, 2004):

$$i_{thz} = P_{in} V_b \frac{\eta e \lambda \mu \tau_c}{h c l^2} (1 + \omega^2 \tau_c^2)^{-\frac{1}{2}} \tag{1}$$

where λ is the optical source wavelength, c is the speed of light, h is Planck's constant, l is the electrode distance, P_{in} is the total optical input power, V_b is the bias voltage, η is the quantum efficiency of the optical absorption process, e is the elementary charge, τ_c is the average carrier lifetime, and μ is the photocarrier mobility in the ultrafast semiconductor. The radiated output power from an antenna is given by (Balanis, 2005), p. 82:

$$P_{rad} = i^2 r_{rad} \tag{2}$$

where i is the rms current into the antenna terminals and r_{rad} is the radiation resistance, which is the part of the input resistance actually giving rise to radiation.

We now use the known dimensions and the experimental results for the D1-D3 dipole photomixers with identical photoconductors from (Duffy et al, 2001) to obtain an estimate of the photocurrent. The peak output power of the D1-D3 designs have been measured experimentally as $3\,\mu$W at 0.85 THz, $2\,\mu$W at 1.05 THz and $0.5\,\mu$W at 1.6 THz. We performed a numerical simulation of the D1-D3 radiation resistances using CST Microwave Studio® 2013. The frequency domain solver was chosen for the task along with a tetrahedral mesh with adaptive mesh refinement due to its suitability for inclusion of smaller features in an otherwise electrically large structure. The 1 μm LT GaAs layer is not modelled separately from the highly resistive GaAs bulk substrate ($\varepsilon_r = 12.94$) in the simulation, as the low temperature growth and subsequent annealing only gives rise to a limited change ($\Delta n \simeq 0.25$) in refractive index (Dankowski et al, 1994), and consequently, the dielectric constant. The substrate is assumed lossless, due to the annealing of the LT GaAs layer and an otherwise highly resistive GaAs base layer (Blakemore, 1982). The poorly conducting Ti adhesion layer has not been modelled, and only the Au thickness has been accounted for in the simulations. The Au conductor loss has been modelled by manually entering the data points for frequency dependent surface resistance, obtained using a Drude model in accordance with the recommendation from (Lucyszyn, 2003). Port parasitics were modelled with 0.75 fF excess capacitance and the excitation was performed with an infinite impedance current port. When driving the D1 structure with a port current of 145 μA, we obtain a radiated power of approximately 3 μW at 0.85 THz.

Figure 1 shows the calculated AC photocurrent i_{thz} using equation (1) at $\omega_{ref} = 2\pi \cdot 0.85$ THz, where the average photocarrier lifetime is $\tau_c = 300$ fs (Duffy et al, 2001), mobility value is $\mu = 0.01$ m^{2}V^{-1}s^{-1} (Brown, 2003), an optical source wavelength of $\lambda = 850$ nm, and an electrode gap of $l = 0.8$ μm (Duffy et al, 2001)

for an optical power range from 0 to 35 mW and a bias voltage range from 0 to 15 V. One possible way of obtaining $i_{thz,ref} = 145\,\mu$A, as predicted by CST
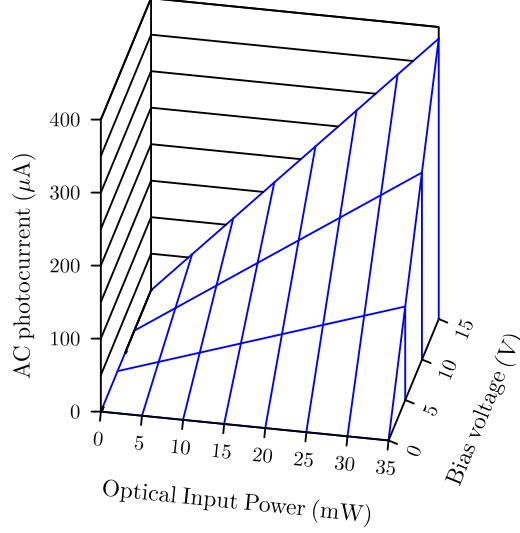

Fig. 1 Calculated AC photocurrent of an LT GaAs photoconductor at 0.85 THz with $\mu = 0.01$ m^{2}V^{-1}s^{-1}, $\tau_c = 300$ fs, $\eta = 0.43$, and $l = 0.8\,\mu$m using 850 nm optical sources.

Microwave Studio®, is to use the combination of an optical input power $P_{in} = 20$ mW and a bias voltage $V_b = 10$ V.

We can now calculate the radiated output power P_{rad} for any given frequency, ω, using equation (2):

$$P_{rad} = r_{rad}\, i_{thz}^2 = r_{rad}\frac{i_{0,ref}^2}{1 + \omega^2\tau_c^2} \qquad (3)$$

where $i_{0,ref}$ is the normalised photocurrent, without the influence of the bandwidth limiting average carrier lifetime, τ_c: $i_{0,ref} = i_{thz,ref}\sqrt{1 + \omega_{ref}^2\tau_c^2}$. Using $\tau_c = 300$ fs, $\omega_{ref} = 0.85$ THz and $i_{thz,ref} = 145\,\mu$A we get $i_{0,ref} = 274\,\mu$A. The radiation resistance, r_{rad}, for D1 to D3 is found by dividing the radiated power, $P_{rad,sim}$ with the square value of the port current, $i_{port,sim}$.

This allows us to directly calculate the predicted power levels of the simulated structures using the material properties from (Duffy et al, 2001) and equation (3). Figure 2 shows the simulation results for the photomixers D1-D3 by applying our method. Data points for actual measurements have been superimposed and show good coherence between the experiment of (Duffy et al, 2001) and our simulations.
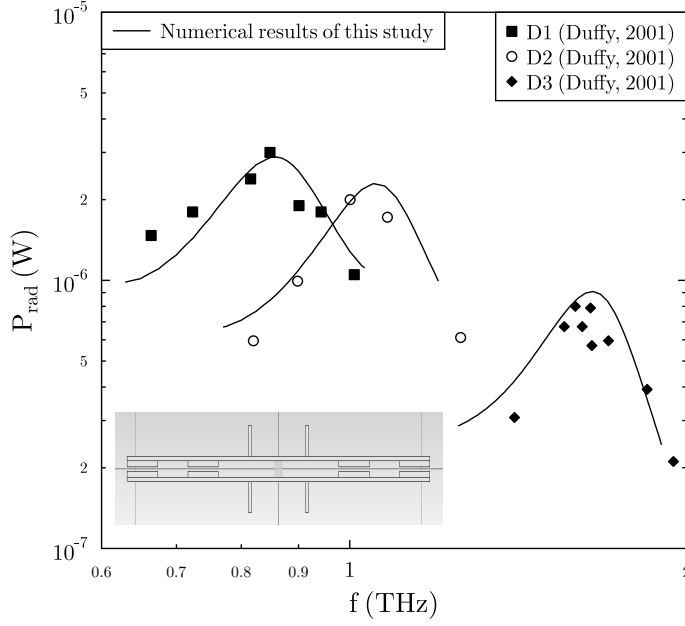
Fig. 2 Numerical results for the output power P_{rad} of the dual dipoles D1-D3 from (Duffy et al, 2001) though application of our simulation method with experimentally measured power levels superimposed. Inset: D1 photomixer simulation model.

3 Numerical Results and Discussion

Next, we propose our two new solutions, Design I and Design II, based on the T-match antenna by (Kraus and Sturgeon, 1940) each with two options, a uniplanar metal-semiconductor-metal (MSM) structure or a multilayer stack, for the DC-blocking structures.

The T-match antenna is a classical antenna structure which features a higher input resistance, as a result of multiple simultaneous radiating elements, requiring less current to achieve a similar output power compared to that of an equivalent dipole antenna. The antenna consists of a long dipole element with a shorter driving element dipole tapped at the $\lambda/4$ and $3\lambda/4$ points of the larger full wave dipole. According to (Balanis, 2005), p. 532, the input impedance of a lossless wire version of the T-match antenna is approximately:

$$Z_{in} \approx (1 + \alpha^2)Z_a \tag{4}$$

where α is the current division factor between the two dipoles (α is unity in case of equal antenna cross sections) and Z_a is the input impedance of the structure without the T-match connection.

Design I is a photomixer based on the T-match antenna with a $0.3\,\mu$m thick Au planar conductor on a thin Ti adhesive layer on a GaAs substrate with a $1\,\mu$m LT GaAs layer (Figure 3). The antenna dimensions are designed for full wave operation and a DC-blocking MSM finger structure is inserted into the long dipole element, to prevent the photomixer bias supply from encountering a short circuit.
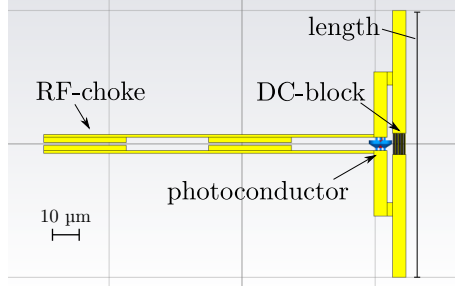
Fig. 3 Design I: Based on a T-match antenna with a uniplanar MSM DC-blocking capacitance.

A $\lambda/4$ RF-choke is added to the design to prevent terahertz current from leaking into the bias supply.

Parameter sweeping results suggests that a conductor width of $5\,\mu$m is a suitable dimension for the structure, allowing for enough MSM area for the DC-block to achieve terahertz AC-conductance. Furthermore, the width allows for an incorporation of a $5\,\mu$m x $5\,\mu$m photoconductor area without discontinuities. The optimum size for the gap between the dipole elements is approximately $2\,\mu$m. The choke segment length is $30\,\mu$m. In order to provide an adequate coupling, the DC-block finger width and spacing must be on the order of 200 nm. The length of the MSM structure is $8\,\mu$m in the direction parallel to the dipoles.

Figure 4 shows the Design I radiated output power for antenna lengths from $96\,\mu$m to $108\,\mu$m, reaching up to $6.7\,\mu$W at 0.85 THz.
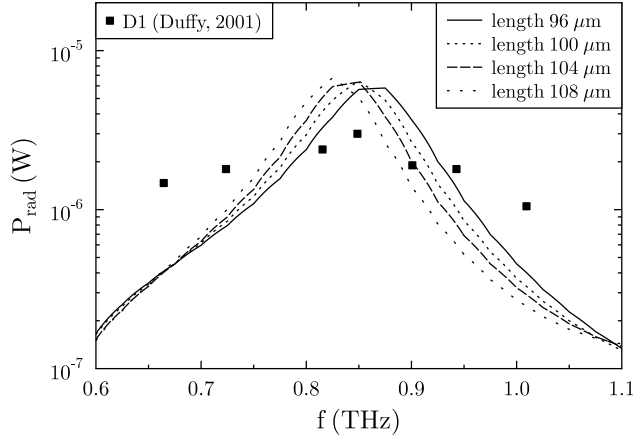

Fig. 4 Numerical results for the radiated output power P_{rad} of Design I with an MSM DC-blocking capacitance.

Design II is developed as follows: The T-match antenna input impedance can be further increased, if an additional long dipole element is placed next to the

driving short dipole element. This can be achieved by mirroring the structure consisting of the long dipole element including the DC-block, the tapping connections, and the RF-choke (Figure 5).
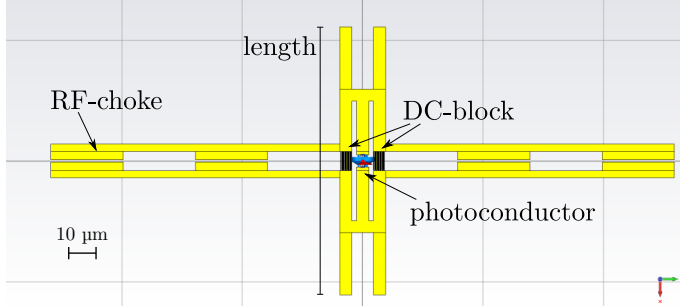

Fig. 5 Design II: An extension of the T-match antenna with an additional long dipole element. Choke and DC-blocks are kept symmetrical

The radiation resistance for Design II with an antenna length from $96\,\mu$m to $111\,\mu$m with uniplanar MSM DC-blocks (Figure 6) is subject to a roll-off beyond 0.7 THz, with an estimated output power at 0.85 THz of $6.0\,\mu$W. The roll-off can be explained by the changed charge distribution on the centre dipole as the proximity effect will have an influence on the charge distribution on the long dipole elements, and consequently in the charge distribution on the MSM, where the current is concentrated near the inner edge along the gap between the dipoles. Adding an additional long dipole element next to the driving dipole element will invariably change the current density of the latter. A changed charge distribution across the MSM will affect its reactive properties and thus its efficacy as a DC-block.

The very fine uniplanar MSM-finger structure used for the DC-blocking may become a challenge to reproduce reliably with good manufacturing yields, when doing lift-off, after mask-based photolithography. E-beam lithography could be a solution, but would also add cost in terms of equipment and manufacturing time. Finally, the fine structures are sensitive to high current densities which increase the risk of early device failure. A more reliable capacitive structure with larger metal cross sections could consist of overlapping conductors separated by a layer of $0.1\,\mu$m silicon nitride. The lower layer conductors are separated by a $1\,\mu$m gap and the whole structure occupies the exact same area ($5\,\mu$m x $8\,\mu$m) as the uniplanar MSM (Figure 7). A structure like this would add additional processing steps for mask alignment and nitride/Au deposition, but would pay off in terms of not requiring the additional cost of an e-beam system and improving device reliability.

The performance of Design I with a multilayer DC-block remains largely unchanged (Figure 8) compared to the MSM-version (Figure 4). The radiated output power stays at $6.7\,\mu$W at 0.85 THz. This suggests that the MSM DC-block works as intended for the Design I layout. Design II with a multilayer DC-block shows a greatly improved radiated output power of $9.0\,\mu$W at 0.85 THz (Figure 9), which is an improvement of 3 times over D1 from (Duffy et al, 2001). The multilayer DC-
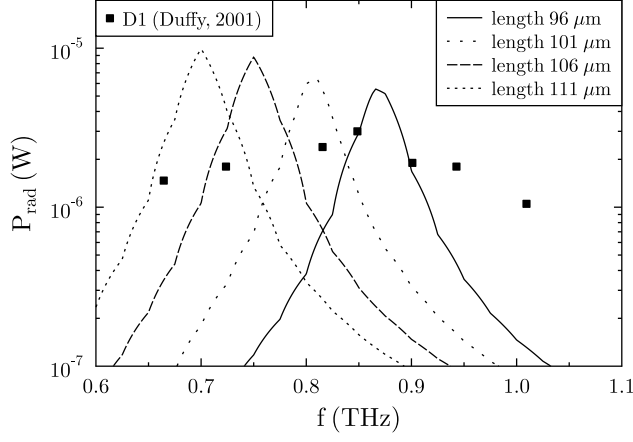
Fig. 6 Numerical results for the radiated output power P_{rad} of Design II with an MSM DC-blocking capacitance.
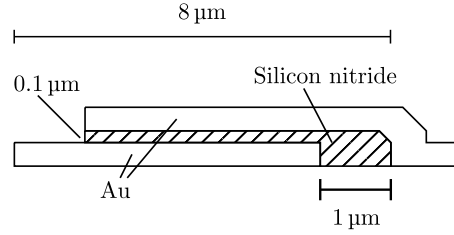

Fig. 7 Cross section of a multilayer DC-blocking structure. The metal layers are separated by a thin nitride layer. The structure occupies the same $5\,\mu$m x $8\,\mu$m surface area as the MSM DC-block

block supplies a large enough reactance, such that it becomes invariant towards the current distribution on the centre dipole.

4 Conclusion

This work has presented a way of estimating photomixer output power levels by applying our simulation methodology to determine the radiation resistance of a known photomixer with measured output power results in order to find the photoconductor THz ac-current. This allows for output power prediction for new photomixer structures simulated with similar features in terms of photoconductor layout, substrate dielectric constant, and conductor material.

We have delivered two new implementations of the classical T-match antenna, adapted to a planar layout with bias supply DC-blocking. Design I features the
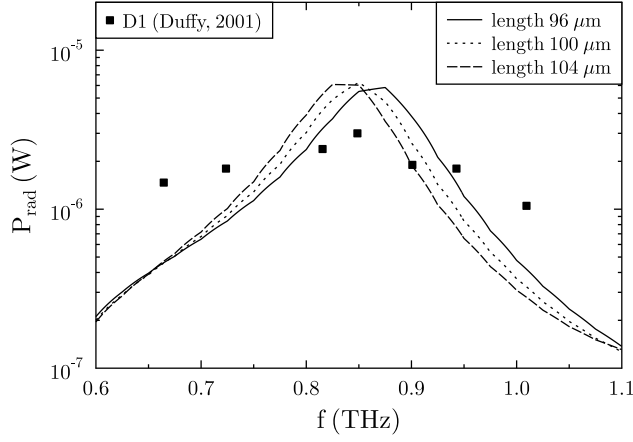
Fig. 8 Numerical results for the radiated output power P_{rad} of Design I with a multilayer DC-block structure.
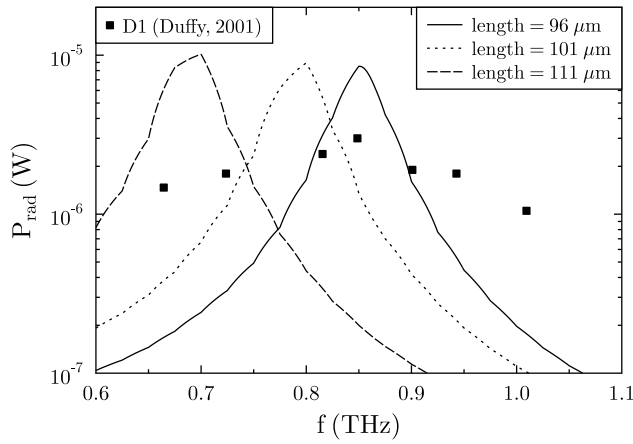

Fig. 9 Numerical results for the radiated output power P_{rad} of Design II with a multilayer DC-blocking capacitance.

classical two conductor approach, and Design II is a novel version of the T-match structure consisting of three conductors. The estimated output power of the Design I photomixer becomes $6.7\,\mu$W at 0.85 THz, compared to $6.0\,\mu$W for the Design II version.

The MSM configuration of the DC-block is thought to be the reason for the unexpected lower performance, which is confirmed by replacing it with a multilayer DC-blocking structure. The performance of Design I with a multilayer DC-block is

unchanged at $6.7\,\mu$W, whereas the Design II photomixer with the multilayer DC-block has an estimated output power of $9.0\,\mu$W This is an improvement of 3 times over the baseline of $3.0\,\mu$W at 0.85 THz from (Duffy et al, 2001). An additional advantage of using multilayer DC-blocks for Design I or II is the improvement in device lifetime as a result of avoiding the current sensitive, narrow 200 nm conductors required for the MSM.

The designs deliberately avoid the use of expensive design features for manufacturability purposes. They can be directly implemented in a range of GaAs technologies and adapted for other devices with different substrate materials, where a high impedance antenna is needed for THz sources with a weak current drive.

Acknowledgments

References

Asada M, Suzuki S (2013) Compact THz oscillators with resonant tunneling diodes and application to high-capacity wireless communications

Brown ER (2003) THz generation by photomixing in ultrafast photoconductors. International Journal of High Speed Electronics and Systems, 13(2):497–545

Balanis CA (2005) Antenna Theory, 3rd edn. John Wiley & Sons

Blakemore JS (1982) Semiconducting and other major properties of gallium arsenide. Journal of Applied Physics , vol.53, no.10, R123

Dankowski SU, Kiesel P, Knupfer B, Kneissl M, Dohler GH, Keil UD, Dykaar DR, Kopf RF (1994) Annealing induced refractive index and absorption changes of lowtemperature grown GaAs. Applied Physics Letters , vol.65, no.25, pp.3269–3271

Drouin BJ, Pearson JC, Shanshan Y, Gupta H (2013) Characterization and Use of a 1.3-1.5 THz Multiplier Chain for Molecular Spectroscopy. Terahertz Science and Technology, IEEE Transactions on , vol.3, no.3, pp.314–321

Duffy SM, Verghese S, McIntosh KA, Jackson A, Gossard AC, Matsuura S (2001) Accurate modelling of dual dipole and slot elements used with photomixers for coherent terahertz output power. IEEE Transactions on Microwave Theory and Techniques 49(6):1032–1038

Han K, Nguyen T, Park I, Han H (2010) Terahertz yagi-uda antenna for high input resistance. Journal of Infrared, Millimeter and Terahertz Waves 31:441–454

Juul L, Mikulics M, Marso M (2012) Improving output power of terahertz heterodyne photomixer by impedance matching. In: 2012 Ninth International Conference on Advanced Semiconductor Devices & Microsystems (ASDAM)

Kumar S, Chan CWI, Hu Q, and Reno JL (2011) A 1.8-THz quantum cascade laser operating significantly above the temperature of $\hbar\omega$/kB. Nature Phys. vol.7, no.2, pp. 166–171

Köhler R, Tredicucci A, Beltram F, Beere H, Linfield E, Davies A, Ritchie D, Iotti R, Rossi F (2002) Terahertz semiconductor-heterostructure laser. Nature 417(6885):156–159

Kraus JD, Sturgeon SS (1940) The t-matched antenna. QST 9:24–25

Li L, Chen L, Zhu J, Freeman J, Dean P, Valavanis A, Davies A, Linfield E (2014) Terahertz quantum cascade lasers with >1 W output powers. Electronics Letters 50(4):309–311

Lucyszyn S (2003) Accurate CAD modelling of metal conduction losses at terahertz frequencies. Electron Devices for Microwave and Optoelectronic Applications, 2003. EDMO 2003. The 11th IEEE International Symposium on , pp.180–185

Mayorga IC, Mikulics M, Schmitz A, Van der Wal P, Gusten R, Marso M, Kordos P, Luth H (2004) An optimization of terahertz local oscillators based on LT-GaAs technology. Proc. SPIE 5498, Millimeter and Submillimeter Detectors for Astronomy II, pp. 537 –547

Mikulics M (2004) Preparation and optimization of low-temperature-grown GaAs photomixers. PhD thesis, Rheinisch-Westfälische Technische Hochschule Aachen

Mikulics M, Marso M, Stancek S, Michael EA, Kordos P (2006) Terahertz-Radiation Photomixers on Nitrogen-Implanted GaAs. Advanced Semiconductor Devices and Microsystems ASDAM '06 International Conference on, pp.117–120, Oct. 2006

Missous M, Kostakis I, Saeedkia D (2013) Long Wavelength Low Temperature Grown GaAs and InP-Based Terahertz Photoconductors Devices. Sensors Journal, IEEE , vol.13, no.1, pp.63–71

Ravaro M, Jagtap V, Santarelli G, Sirtori C, Li LH, Khanna SP, Linfield EH, and Barbieri S (2013) Continuous-wave coherent imaging with terahertz quantum cascade lasers using electro-optic harmonic sampling. Applied Physics Letters, 102, 091107

Rouvalis E, Renaud CC, Moodie DG, Robertson MJ, Seeds AJ (2010) Traveling-wave uni-traveling carrier photodiodes for continuous wave THz generation. Optics Express, vol.18(11), pp. 11105–11110

Schmielau T, Pereira M (2009a) Impact of momentum dependent matrix elements on scattering effects in quantum cascade lasers. Physica Status Solidi (B) Basic Research 246(2):329–331

Schmielau T, Pereira M (2009b) Momentum dependent scattering matrix elements in quantum cascade laser transport. Microelectronics Journal 40(4-5):869–871

Schmielau T, Pereira M (2009c) Nonequilibrium many body theory for quantum transport in terahertz quantum cascade lasers. Applied Physics Letters 95(23)

Wacker A, Lindskog M, Winge D (2013) Nonequilibrium Green's function model for simulation of quantum cascade laser devices under operating conditions. IEEE Journal on Selected Topics in Quantum Electronics 19(5)